Electronic Supplementary Information

Crystal water for high performance layered manganese oxide cathodes in aqueous rechargeable zinc batteries

Kwan Woo Nam,[‡a] , Heejin Kim,[‡b] Jin Hyeok Choi,[c] and Jang Wook Choi[*d]

[a]Graduate School of Energy Environment Water and Sustainability, Korea Advanced Institute of Science and Technology, 291 Daehak-ro, Yuseong-gu, Daejeon 34141, Republic of Korea

[b]Electron Microscopy Research Center, Korea Basic Science Institute, 169-148 Gwahak-ro, Yuseong-gu, Daejeon 34133, Republic of Korea

[c]KEPCO Research Institute, Korea Electric Power Corporation, 105 Munji-ro, Yuseong-gu, Daejeon 34056, Republic of Korea

[d]School of Chemical and Biological Engineering and Institute of Chemical Process, Seoul National University, 1 Gwanak-ro, Gwanak-gu, Seoul 08826, Republic of Korea

E-mail: jangwookchoi@snu.ac.kr

‡These two authors contribute equally to this work.

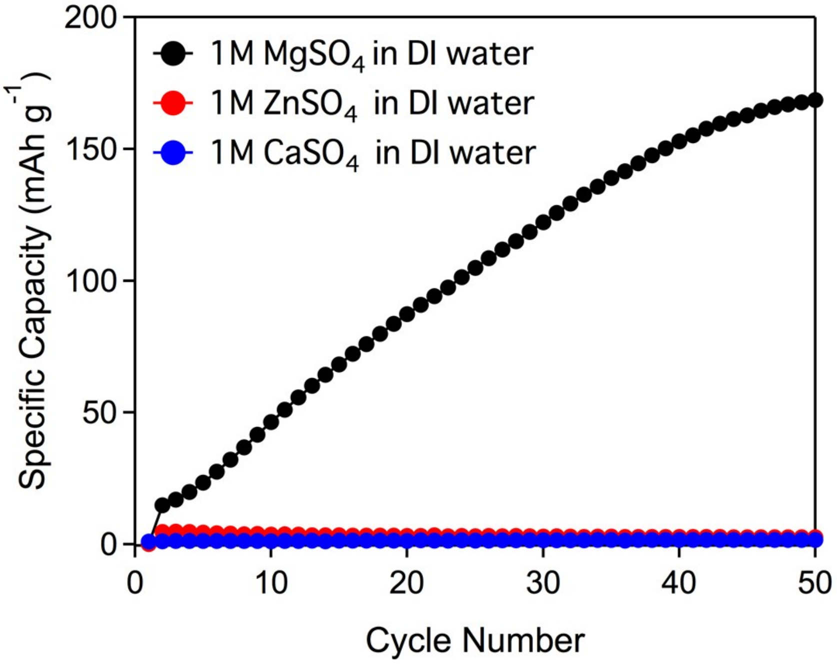

Fig. S1 Monitoring the activation of *cw*-MnO_2 with different divalent ions: Mg^{2+}, Zn^{2+}, and Ca^{2+}.

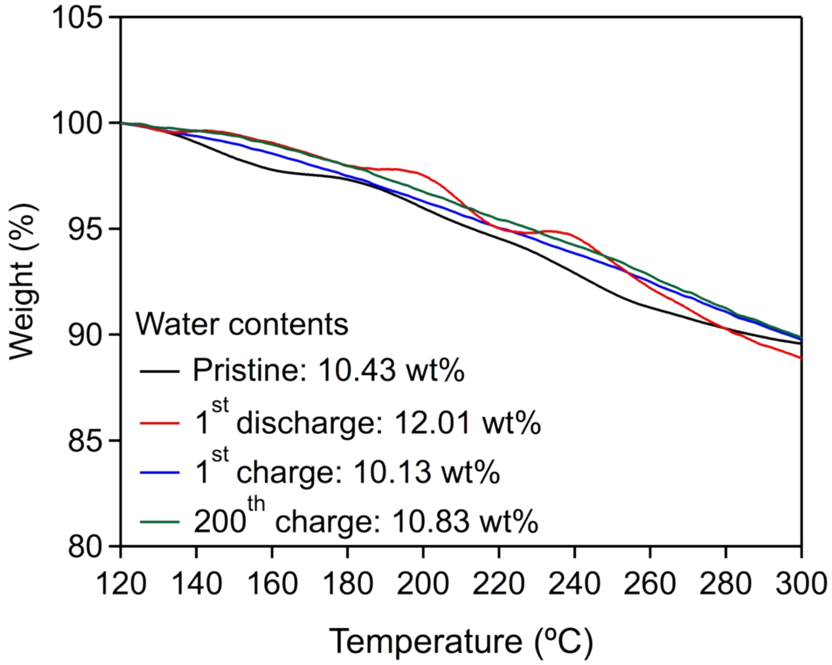

Fig. S2 TGA profiles for the pristine and cycled *cw*-MnO_2.

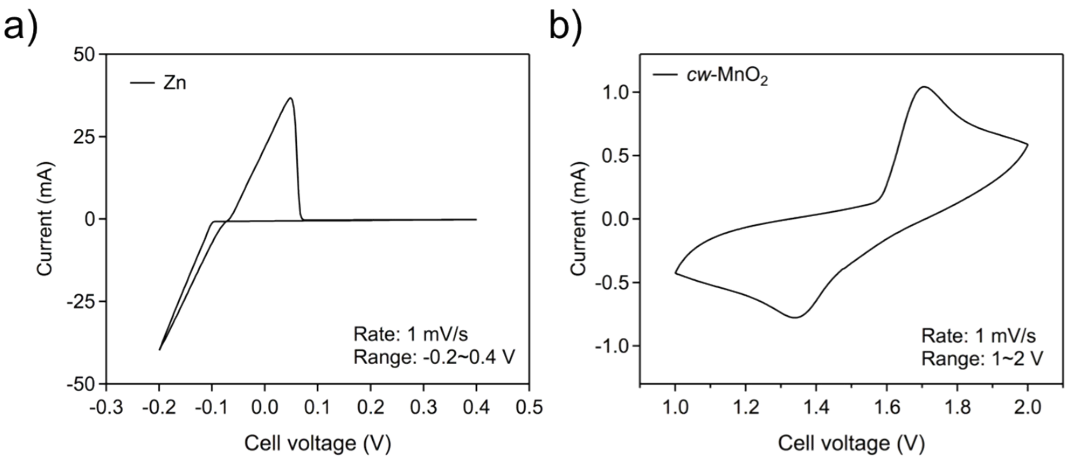

Fig. S3 CVs of a) Zn metal anode and b) *cw*-MnO_2 cathode at a rate of 1 mV s^{-1}. Electrolyte: 1 M $ZnSO_4$ in DI water.

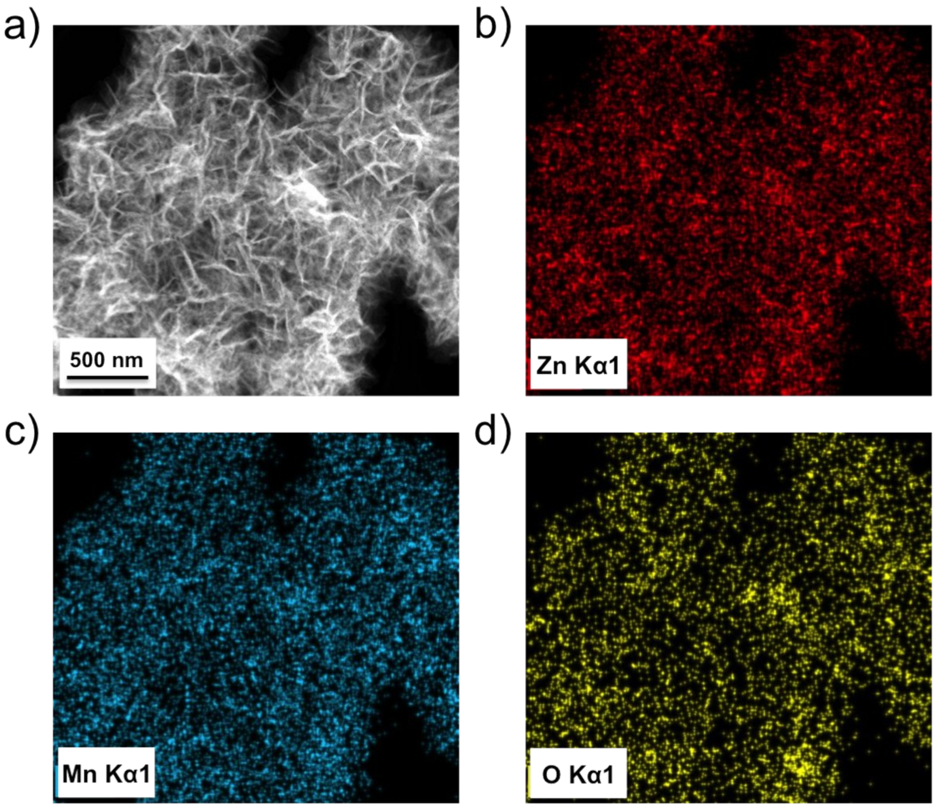

Fig. S4 a) STEM image of the fully discharged *cw*-MnO_2 alongside its EDS elemental mapping with respect to b) Zn, c) Mn, and d) O, suggesting uniform Zn insertion over the electrode.

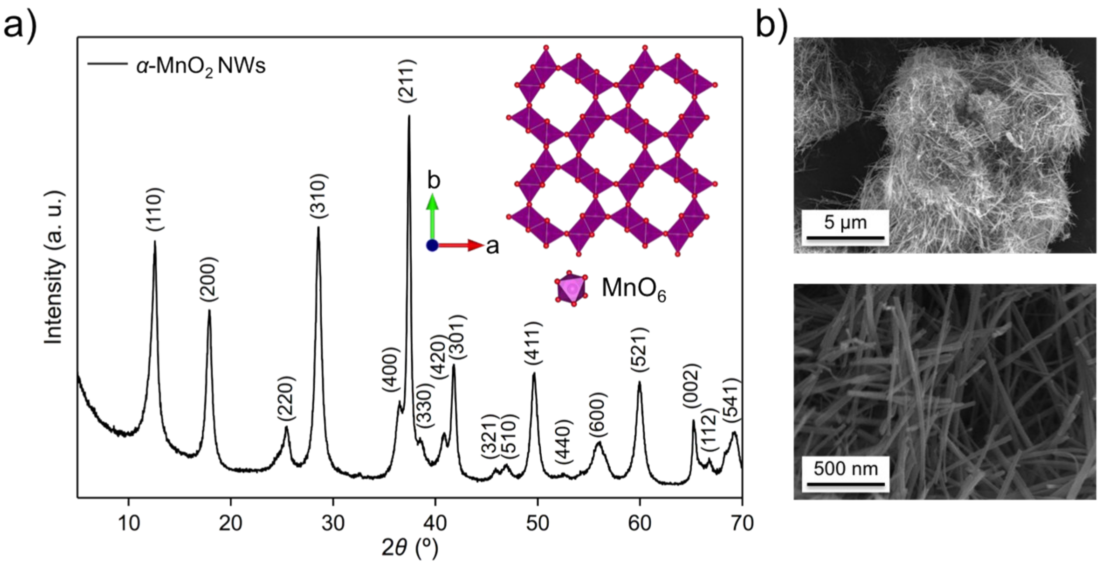

Fig. S5 a) XRD pattern and (inset) crystal structure of α-MnO_2 NWs, and their b) SEM (upper) and TEM (lower) images.

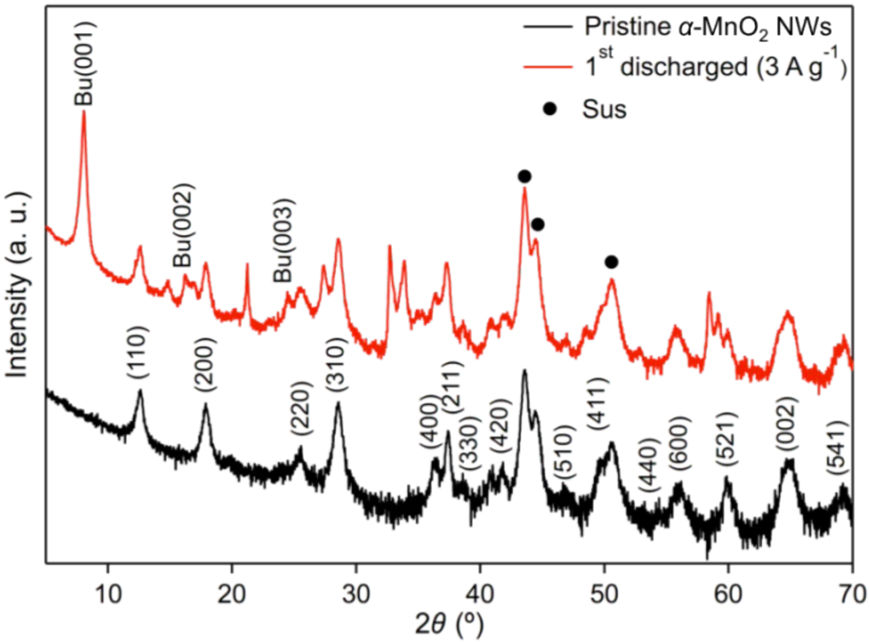

Fig. S6 XRD patterns of α-MnO_2 NWs at the pristine and 1st fully discharged states when scanned at a rate of 3000 mA g^{-1}.

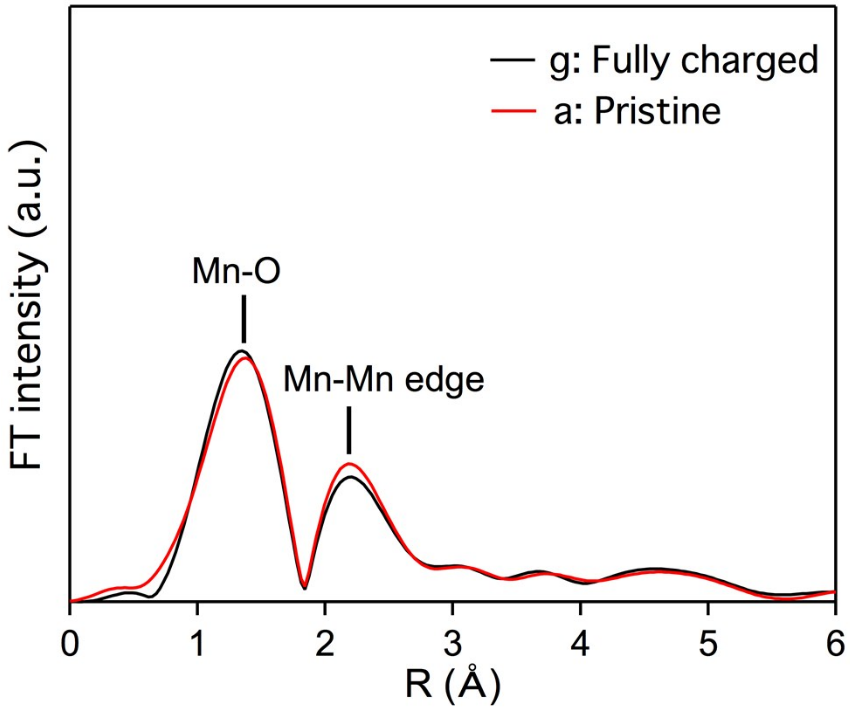

Fig. S7 EXAFS spectra of *cw*-MnO_2 at the pristine and 1st fully charged states.

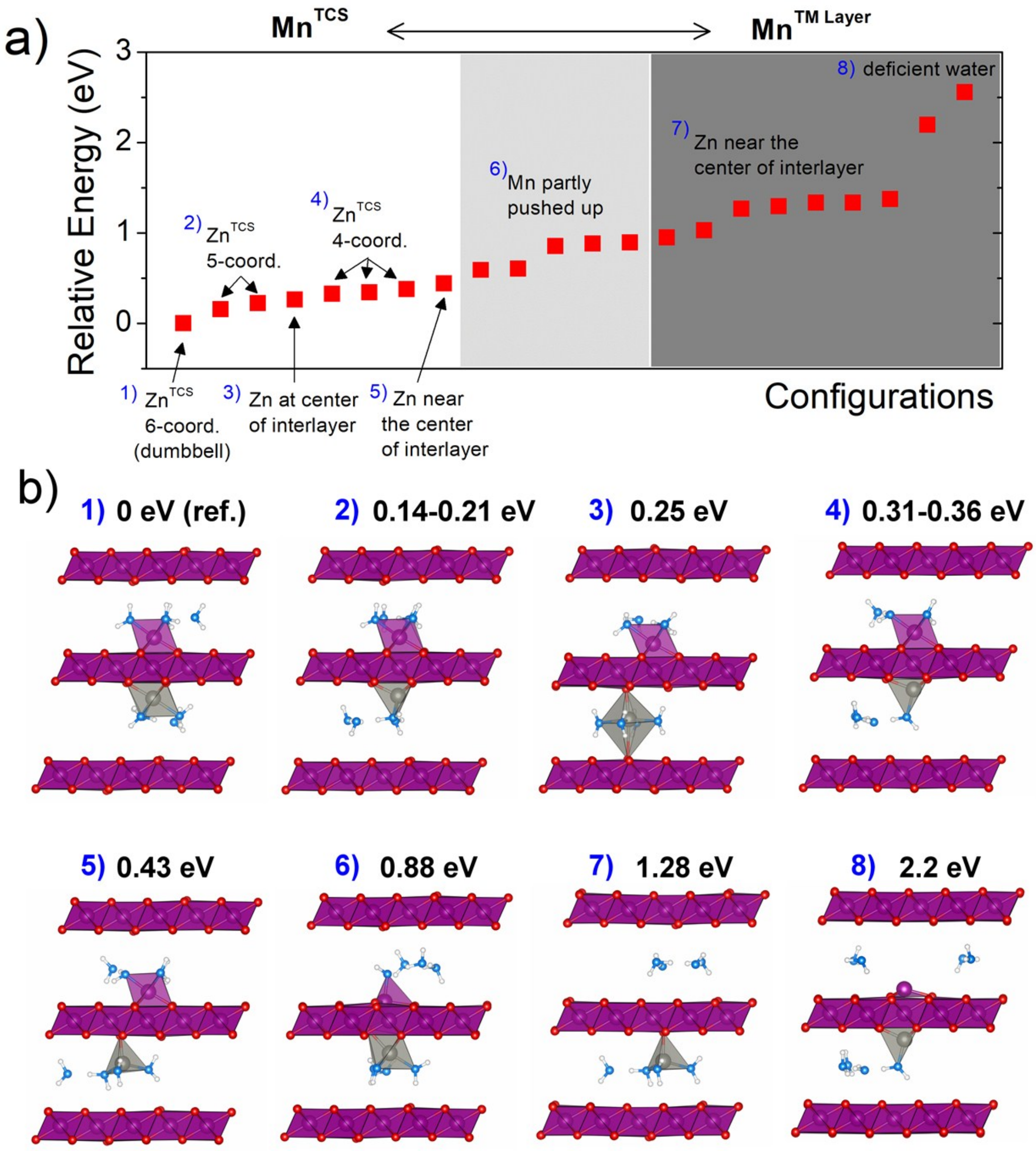

Fig. S8 (a) Relative energy values of various Zn intercalation configurations. Representative structures are illustrated in (b). Purple, red, gray, and white spheres represent Mn, O, Zn, and H, respectively. Blue sphere is O of crystal water molecule. Numbers are relative energy in eV in reference to the most stable structure (configuration 1).

Note. Overall, the environment of Mn is more critical for the total energy compared to that of Zn, which implies that Mn is more sensitive to its coordination than Zn is. When Zn is adsorbed, Mn favors the triple-corner-sharing (TCS) sites (left side of Figure S8a) due to the repulsion from Zn. For the same Mn configurations, Zn prefers the TCS site (configurations 1, 2, and 4) at first, followed by the center of the interlayer space (configuration 3). Without protruding Mn, Zn occupies the center of the interlayer space (configuration 7). When the amount of crystal water is insufficient so that the protruding Mn could not be coordinated by water, the system is highly unstable (configuration 8), reflecting the critical role of crystal water for stabilizing the discharged state.

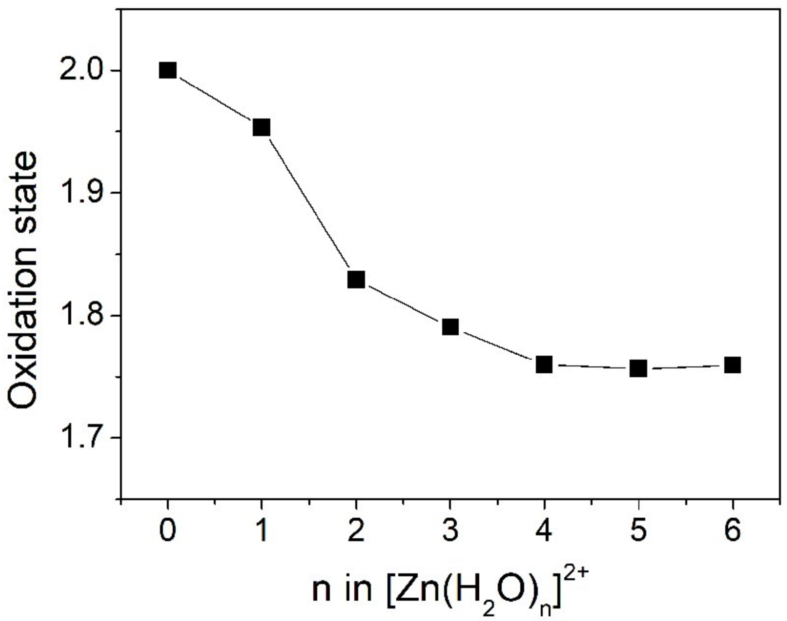

Fig. S9 Oxidation state of Zn center as a function of the number of coordinate water molecules. The extent of charge transfer from ligand water to Zn center converges to ~0.25 for n = 4, 5, and 6.

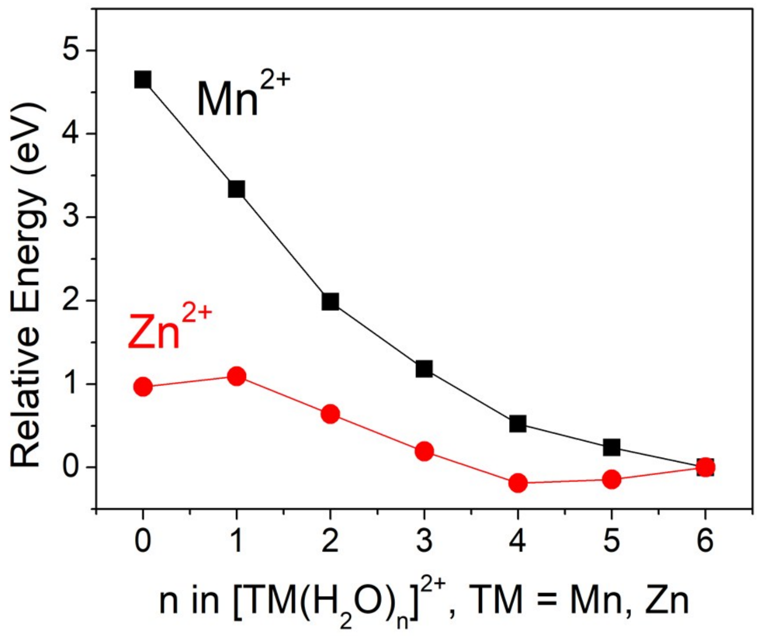

Fig. S10 Relative energies of Mn^{2+} and Zn^{2+} cations as a function of the number of coordinate water molecules. Octahedral complexes (n = 6) are used as a respective reference.

Note. Molecular calculations were performed by using the B3LYP functional[1] with 6-31+g** basis set and Grimme's D3 dispersion correction (zero damping),[2] as implemented in the Q-Chem software package.[3] Solvent effects were considered by applying the universal continuum solvation model (SM8).[4]

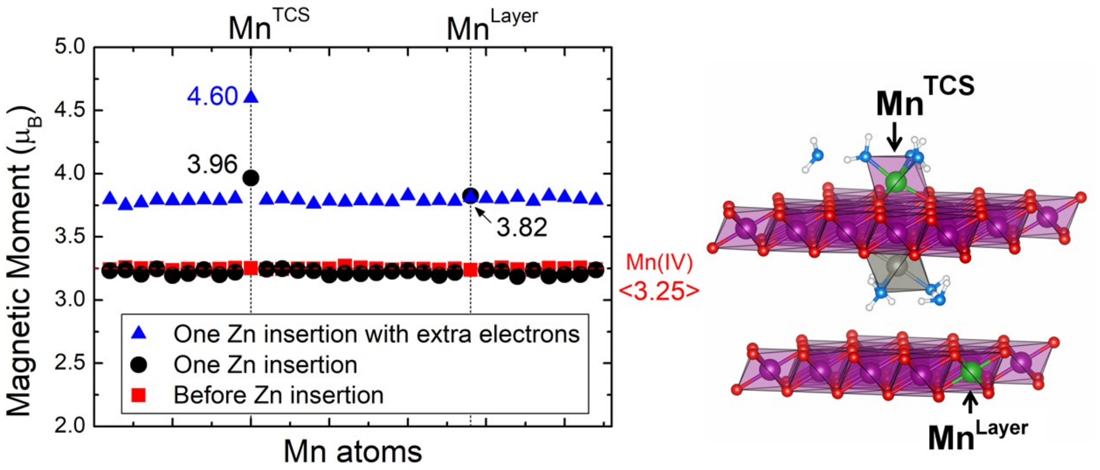

Fig. S11 Net magnetic moments of Mn atoms before and after the Zn insertion. Before the Zn ion insertion (red square), average net moment is 3.25, which corresponds to the Mn^{4+} state. Upon the one Zn ion insertion (black circle), two kinds of Mn atoms (Mn^{TCS} and Mn^{Layer} as illustrated with green spheres in the right panel) are available for reduction. Between them, the one in the dumbbell complex (Mn^{TCS}) undergoes a larger change in the magnetic moment (to 3.96), implying that the given Mn is more likely reduced upon the Zn ion insertion. With supplying extra electrons (blue triangle), Mn^{TCS} is further reduced to Mn^{2+} ahead of other Mn in the TM layer. For the latter calculation, 31 extra electrons were supplied to the $Zn_1Mn_{32}O_{64}$ structure to make one type of Mn reduced to Mn^{2+}. The purple and green spheres represent Mn^{4+} and reduced Mn atoms, respectively. Grey, red, blue, and white spheres represent Zn, crystal O, water O, and hydrogen, respectively.

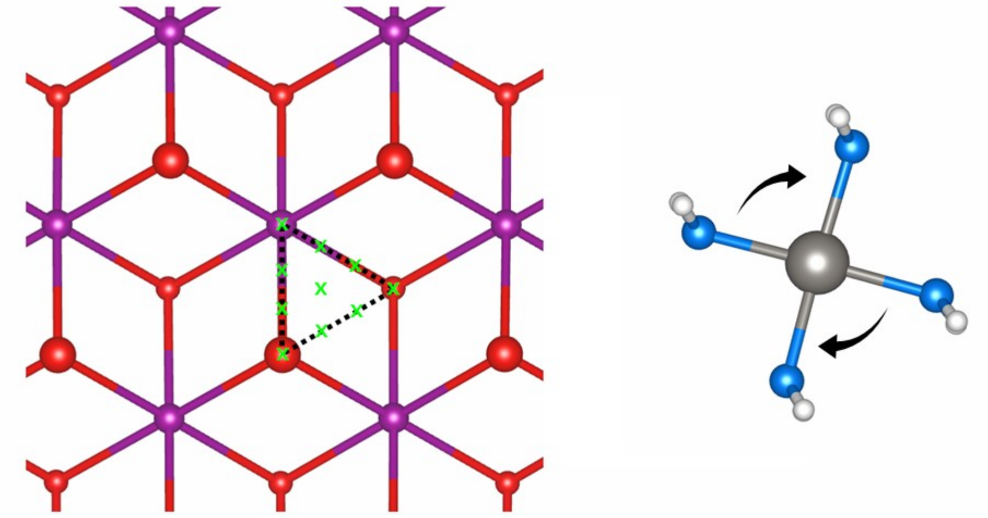

Fig. S12 Initial positions of Zn ion to obtain the potential energy surface in the interlayer space. The $Zn(H_2O)_4$ complex (right panel) was progressively translated to each grid point (green crosses in the left panel) and rotated from 0˚ to 60˚ by 15˚ at each position to explore the stable geometries. As a result, 50 initial configurations were identified, and they were optimized by relaxing the water molecules and z position of Zn ion, while constraining the other degrees of freedom (x and y position of Zn and the entire MnO_2 framework). The red and violet balls in the left panel represent O and Mn, respectively.

Table S1. ICP analysis of the dissolved Mn in electrolyte.

State	Mn in electrolyte		
	[ppm]	[µmol]	Dissolved portion [%] in reference to total Mn
1st discharge	0	0	0
1st charge	9.40	0.17	0.74
100th charge	42.29	0.77	3.35
200th charge	43.02	0.78	3.40

References

1 A. D. Becke, *J. Chem. Phys.*, 1993, **98**, 5648-5652.

2 D. G. A. Smith, L. A. Burns, K. Patkowski and C. D. Sherrill, *J. Phys. Chem. Lett.*, 2016, **7**, 2197-2203.

3 Y. Shao, Z. Gan, E. Epifanovsky, A. T. B. Gilbert, M. Wormit, J. Kussmann, A. W. Lange, A. Behn, X. Feng, D. Ghosh, M. Goldey, P. R. Horn, L. D. Jacobson, I. Kaliman, R. Z. Khaliullin, T. Kuś, J. Liu, E. I. Proynov, Y. M. Rhee, R. M. Richard, A. Rohrdanz, R. P. Steele, E. J. Sundstrom, H. L. W. Iii, M. Zimmerman, D. Zuev, B. Albrecht, E. Alguire, B. Austin, G. J. O. Beran, Y. A. Bernard, E. Berquist, K. Brandhorst, B. Bravaya, S. T. Brown, D. Casanova, C.-m. Chang, S. H. Chien, K. D. Closser, D. L. Crittenden, R. A. D. Jr, H. Do, A. D. Dutoi, G. Edgar, S. Fatehi, L. Fusti-molnar, A. Ghysels, A. Golubeva-, J. Gomes, M. W. D. Hanson-heine, H. P. Philipp, A. W. Hauser, E. G. Hohenstein, Z. C. Holden, T.-c. Jagau, H. Ji, B. Kaduk, K. Khistyaev, J. Kim, J. Kim, R. A. King, P. Klunzinger, D. Kosenkov, T. Kowalczyk, C. M. Krauter, K. U. Lao, A. D. Laurent, K. V. Lawler, V. Levchenko, C. Y. Lin, F. Liu, E. Livshits, R. C. Lochan, A. Luenser, P. Manohar, S. F. Manzer, S.-p. Mao, A. V. Marenich, S. A. Maurer, N. J. Mayhall, E. Neuscamman, C. M. Oana, R. Olivares-amaya, P. O. Neill, J. A. Parkhill, T. M. Perrine, R. Peverati, D. R. Rehn, E. Rosta, N. J. Russ, S. M. Sharada, S. Sharma, D. W. Small, A. Sodt, T. Stein, D. Stück, Y.-c. Su, A. J. W. Thom, T. Tsuchimochi, V. Vanovschi, O. Vydrov, T. Wang, M. A. Watson, J. Wenzel, A. White, C. F. Williams, J. Yang, S. Yeganeh, S. R. Yost, I. Y. Zhang, X. Zhang, Y. Zhao, B. R. Brooks, K. L. Chan, D. M. Chipman, C. J. Cramer, W. A. Goddard, M. S. Gordon, W. J. Hehre, A. Klamt, H. F. S. Iii, M. W. Schmidt, C. D. Sherrill, D. G. Truhlar, A. Warshel, X. Xu, A. Aspuru-guzik, R. Baer, A. T. Bell, N. A. Besley, D. Chai, A. Dreuw, B. D. Dunietz, T. R. Furlani, R. Steven, C.-p. Hsu, Y. Jung, J. Kong, D. S. Lambrecht, W. Liang, C. Ochsenfeld, V. A. Rassolov, V. Lyudmila, J. E. Subotnik, T. V. Voorhis, J. M. Herbert, I. Anna, P. M. W. Gill, M. Head-gordon, Y. Shao, Z. Gan, E. Epifanovsky and A. T. B. Gilbert, *Mole. Phys.*, 2015, **113**, 184-215.

4 A. V. Marenich, R. M. Olson, C. P. Kelly, C. J. Cramer and D. G. Truhlar, *J. Chem. Theory Comput.*, 2007, **3**, 2011-2033.